fibers

MDPI

Article

Application of L-Shaped Zigzag Steel Fibers with Different Parameters in Asphalt Mixtures

Qingguo Yang, Wujing Yin *, Jiawei Cheng, Ya Li *, Yu Zhou, Kelin Chen and Yunhao Li

School of Civil Engineering, Chongqing Jiaotong University, Chongqiong 400074, China; 990020020405@cqjtu.edu.cn (Q.Y.); 13271903262@163.com (J.C.); 622230970092@mails.cqjtu.edu.cn (Y.Z.); 17815058793@163.com (K.C.); h13782706283@163.com (Y.L.)

* Correspondence: 622230951053@mails.cqjtu.edu.cn (W.Y.); 990202100033@cqjtu.edu.cn (Y.L.)

Highlights

What are the main findings?

- Compared with ordinary asphalt mixtures, L-shaped steel fibers significantly enhance the comprehensive mechanical properties of asphalt mixtures, improving the overall performance enhancement effect by approximately 20%.
- When the content of L-shaped steel fibers reaches 2%, the asphalt mixture achieves the optimal comprehensive performance.
- The data dispersion was characterized by standard deviation and coefficient of variation. Results indicated that data related to L-shaped steel fibers exhibited smaller relative fluctuations, suggesting a higher degree of uniformity and stability.

What is the implication of the main finding?

- The incorporation of L-shaped steel fibers can effectively improve the performance of asphalt mixtures, enhancing their high-temperature stability, low-temperature crack resistance, and water stability. This is of great significance for enhancing the service performance of asphalt pavements.
- Compared with straight steel fibers, L-shaped steel fibers have more advantages in improving the performance of asphalt mixtures, providing a reference for the selection of appropriate steel fiber types in practical engineering.
- The optimal comprehensive dosage of L-shaped steel fibers was determined to be 2%, providing specific parameter basis for the rational application of L-shaped steel fibers in practical engineering projects.
- The low data dispersion and high uniformity stability of L-shaped steel fibers indicate that they are evenly distributed within the asphalt mixture. This even distribution contributes to the assurance of the performance stability of the asphalt mixture and is beneficial for the control of engineering quality.

Abstract: Taking AC-13 asphalt mixture as the matrix, this research delves into the impacts of assorted steel fibers on AC-13 asphalt mixture, especially the influence of 17.5 mm × 17.5 mm L-shaped steel fibers. A gradient design with mass dosages of 0%, 1%, 2%, and 3% was employed to evaluate the reinforcement effect of L-shaped steel fiber-reinforced asphalt mixture compared with conventional mixture. Also, comparative analysis between L-shaped and straight steel fibers was conducted through comprehensive mechanical performance tests, including the Marshall stability test, high-temperature wheel tracking test, low-temperature beam bending test, freeze–thaw splitting strength test, and immersion Marshall test. The results demonstrate that L-shaped steel fibers significantly improve the comprehensive mechanical properties of asphalt mixture compared

check for updates

Academic Editor: Messaoud Saidani

Received: 3 April 2025
Revised: 1 May 2025
Accepted: 29 May 2025
Published: 2 June 2025

Citation: Yang, Q.; Yin, W.; Cheng, J.; Li, Y.; Zhou, Y.; Chen, K.; Li, Y. Application of L-Shaped Zigzag Steel Fibers with Different Parameters in Asphalt Mixtures. *Fibers* **2025**, *13*, 71. https://doi.org/10.3390/fib13060071

Copyright: © 2025 by the authors. Licensee MDPI, Basel, Switzerland. This article is an open access article distributed under the terms and conditions of the Creative Commons Attribution (CC BY) license (https://creativecommons.org/licenses/by/4.0/).

to conventional asphalt mixture, showing remarkable improvements in high-temperature stability, low-temperature crack resistance, and water stability. The overall performance enhancement effect increases by approximately 20%. Compared with straight steel fibers, the performance improvement of the mixtures is slightly greater, with the optimal performance achieved at 2% mass dosage. The standard deviation and coefficient of variation are used to reflect the degree of data dispersion. The results show that the data of L-shaped steel fibers have relatively smaller fluctuations, being more uniform and stable.

Keywords: asphalt mixture; L-shaped steel fiber; mechanical properties; reinforcement effect

1. Introduction

Asphalt mixture, being the core material of asphalt pavement structure, directly determines the service quality and service life of the pavement. The mechanical strength of the mixture mainly results from the bonding effect of the asphalt binder and the interlocking friction between the aggregates. When the interfacial bonding performance between the asphalt and the aggregates weakens, or there are pore defects within the mixture, fatigue damage is likely to occur under the repeated action of vehicle loads. This leads to the deterioration of the material strength and subsequently the generation of macroscopic cracks, thereby triggering typical diseases such as rutting and bleeding [1]. When the cohesive force of the mixture decreases and pores exist, the dynamic water pressure in pores and freeze–thaw damage from ice crystals become the main causes of damage in porous asphalt pavement during winter [2]. The reduction in frictional resistance between aggregates can easily lead to a series of pavement issues, including rutting and pushing deformation.

To effectively improve the service performance and durability life of asphalt pavements, adding fiber reinforcement materials to asphalt mixtures has become a common technical means in engineering practice. The incorporation of fibers can significantly improve the crack resistance, rut resistance, and fatigue durability of the mixture.

The incorporation of basalt fibers, glass fibers, natural fibers, polypropylene fibers, and steel fibers into asphalt mixtures can all have a positive impact on the performance of asphalt mixtures and the service performance of pavements. Qin et al. [3] and Wu et al. [4] explored the influence of basalt fibers with different lengths and contents on the properties of asphalt binders. Their findings indicated that basalt fibers create a robust three-dimensional network in the asphalt binder. This network efficiently distributes stress and restrains crack growth, enhancing the binder's overall performance. Piuzzi et al. [5] and Yang et al. [6] conducted in-depth analyses of the reinforcement mechanisms of glass fibers in asphalt mixtures. Their research revealed that augmenting the glass fiber content significantly enhances the stiffness, rutting resistance, creep recovery, and low-temperature cracking resistance of the mixtures. This improvement in key mechanical properties effectively extends the fatigue life of asphalt concrete pavement structures. Pirmohammad et al. [7] and Hojjati et al. [8] investigated the fracture behavior of asphalt mixtures modified with two types of natural fibers. Their findings showed that both fiber modifications significantly improved the fracture strength of the asphalt mixtures. Wang et al. [9] demonstrated that both the length and content of polypropylene fibers significantly enhance the fracture properties of asphalt binders. The main toughening mechanisms are crack bridging and fiber pull-out. Mohd Rodz et al. [10] conducted microstructural analyses of steel fiber-reinforced porous asphalt mixtures, showing that steel fibers significantly enhance the performance of porous asphalt mixtures.

Numerous research studies have shown that steel fibers outperform other fibers in reinforcing asphalt pavements, markedly improving crack resistance, crack propagation patterns, high-temperature performance, and durability. Nian et al. [11] demonstrated that steel fibers effectively enhance the low-temperature crack resistance of recycled asphalt mixtures, thereby improving their durability under cold conditions. Fu et al. [12] evaluated three fiber types using acoustic emission parameters and found that steel fibers promote the conversion of tensile cracks to shear cracks under low-temperature conditions. Yang et al. [13] and Gao et al. [14] investigated the impact of freeze–thaw cycles on the mechanical properties and healing efficiency of fiber-modified asphalt mixtures. Their findings indicated that steel fibers with larger diameters enhanced heating uniformity and demonstrated better fracture resistance than steel wool and carbon fibers. Additionally, these fibers showed reduced vulnerability to moisture and freeze–thaw damage, highlighting their potential for improving the durability of asphalt mixtures. Shapie et al. [15] highlighted steel fibers' significant contribution to pavement durability. Liu et al. [16] and Du et al. [17] investigated the thermal conductivity and self-healing performance of steel fiber-modified asphalt mixtures. Their research validated the material's superior thermal and self-healing properties, underscoring its potential for enhancing pavement durability.

Que et al. [18] highlighted that fiber geometry and spatial arrangement are pivotal in optimizing performance. Kim et al. [19] and Rezakhani et al. [20] modeled the impacts of steel fiber dimensions and geometries on asphalt concrete, demonstrating performance variations that depend on these parameters. Park et al. [21] and García et al. [22] found that longer fibers enhance ductility, while finer, shorter fibers improve high-temperature rutting resistance. Serin et al. [23] and Liu et al. [24] optimized asphalt mixture performance under specific fiber lengths and dosages, reporting significant improvements in rutting resistance, low-temperature cracking resistance, and freeze–thaw durability. Hooked-end fibers demonstrated superior bond strength due to anchoring effects, as confirmed by Abdallah et al. [25] and Mohammed et al. [26]. Wang et al. [27] conducted in-depth analyses of bond–slip behavior in hooked-end and semi-hooked steel fibers, providing insights for geometric optimization. Li et al. [28] and Liu et al. [29] compared pull-out behaviors of hooked-end straight fibers and curved steel fibers, finding curved fibers more effective in reinforcement under identical conditions.

Steel fibers have demonstrated significant advantages in engineering applications due to their remarkable mechanical enhancement effects and durability. Existing research has been predominantly focused on simple-shaped fibers such as straight and hooked-end types. While notable progress has been made in understanding the effects of fiber dimensions, dosage, and basic geometries on composite performance, there remains a conspicuous research gap regarding specifically designed complex-shaped steel fibers. We chose L-shaped fibers for testing because the hooked ends of the L-shape form a mechanical interlocking structure in the mixture. The interfacial bonding mechanism depends on mechanical anchoring and chemical bonding. Compared with straight fibers that only rely on chemical bonding and friction force, their pull-out resistance and stress transfer efficiency are better. During the mixing process, it is easier to form a spatial network, reducing the phenomenon of fiber agglomeration. The uniform dispersion of fibers ensures the feasibility of construction. Based on the limitations of existing research on steel fibers with complex shapes and the urgent need for novel reinforcement materials, we propose the L-shaped folded-line fiber as a reinforcement material for the first time. Its unique geometric shape promotes the interlaced distribution of fibers, enabling a multi-point anchoring mechanism within the asphalt matrix. This distinctive structure can significantly enhance the interfacial bonding strength between the fibers and asphalt, outperforming the single anchoring mode of traditional straight fibers or hooked fibers, owing to its ability to more effectively

transfer stress and resist pull-out forces. This study investigates 17.5 mm × 17.5 mm L-shaped folded steel fibers at three dosages (1%, 2%, and 3%) through multi-dimensional performance tests. The effects on high-temperature rutting resistance, low-temperature cracking resistance, deformation resistance, load-bearing capacity, water damage resistance, and freeze–thaw cycle resistance are evaluated in comparison to mixtures containing 35 mm straight steel fibers and plain asphalt mixtures.

2. Experimental Preparation for Performance Study of Steel Fiber Reinforced Asphalt Mixture

2.1. Materials

1. Asphalt

In this experiment, the Zhongmao Brand SBS (Styrene–Butadiene–Styrene Triblock Copolymer) modified asphalt was provided by Maoming Weilong Petrochemical Co., Ltd., Maoming City, Guangdong Province, China. All test standards GB and GB/T are derived from *Technical Specifications for Construction of Highway Asphalt Pavements (JTG F40-2004)* [30]. Its technical indicators are shown in Table 1.

Table 1. Technical indicators of asphalt.

Test Items	Test Results	Specification Requirements	Test Methods
Softening Temperature (%)	78	≥60	GB/T4507
Plastic Deformation Capacity (cm)	26.3	≥20	GB/T4508
Needle Penetration Depth (1/10 mm)	51.4	40–60	GB/4509
Absolute Viscosity (pa.s)	2.1	≤3	Viscometer method
Flash Point (°C)	281	≥230	GB/T267
Dissolution Capacity (%)	99.5	≥99	GB/T11148
Segregation, Softening Point Difference (°C)	1.8	≤2.5	T0660-98

2. Coarse Aggregates

The coarse aggregates used in this test are crushed basalt stones, which are provided by Langfang Lüxiang Environmental Protection Technology Co., Ltd., Langfang City, Hebei Province, China. The performance metrics are listed in Table 2.

Table 2. Technical indicators of coarse aggregates.

Test Items	Particle Size	Test Results	Specification Requirements	Test Methods
Apparent Relative Density	10–15 mm 5–10 mm 3–5 mm	2.841 2.834 2.837	≥2.5	T0304
Water Absorption Rate (%)	10–15 mm 5–10 mm 3–5 mm	0.53 0.56 0.64	≤3.0	T0304
Stone Crushing Value (%)		17.3	≤28	T0316
Los Angeles Abrasion Loss (%)		20.1	≤30	T0317
Content of Flaky and Elongated Particles (%)		3.1	≤20	T0312

3. Fine aggregate

The fine aggregates used in this test are natural river sands, which are provided by Langfang Lüxiang Environmental Protection Technology Co., Ltd., Langfang City, Hebei Province, China. The performance metrics are listed in Table 3.

Table 3. Technical indicators of fine aggregates.

Test Items	Test Results	Specification Requirements	Test Methods
Apparent Relative Density	2.741	≥2.5	T0316
Water Absorption Rate (%)	1.34	≤3.0	T0317
Content of Particles Smaller than 0.075 mm by Water Washing Method (%)	0.31	≤1.0	T0333

4. Mineral powder

The mineral powder used in this test is slag powder, which is provided by Henan Hengyuan New Materials Co., Ltd., Xinyang City, Henan Province, China. The performance metrics are listed in Table 4.

Table 4. Technical indicators of mineral powder.

Test Items		Test Results	Specification Requirements	Test Methods
Apparent Specific Gravity		2.81	≥2.8	T0352
Hydrophilic Coefficient		0.75	≤1	T0353
Water Content (%)		0.42	≤1	T0103
Appearance		Anti-caking	Anti-caking	
Particle Size Range	<0.6 mm	100	100	T0351
	<0.15 mm	93.2	90–100	
	<0.075 mm	88.1	75–100	

5. Steel fiber

The steel fibers used in this test are plain carbon steel fibers, which are supplied by Hengshui Pufang Steel Fiber Factory, Hengshui City, Henan Province, China. The performance metrics are listed in Table 5.

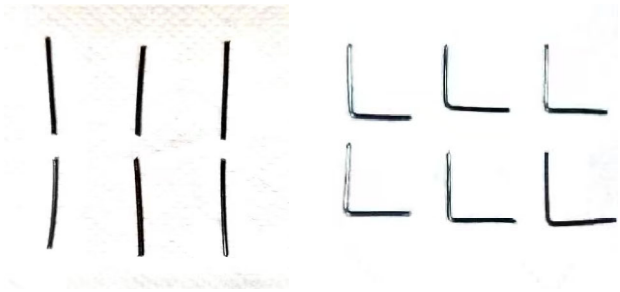
Table 5. Technical indicators of steel fibers.

Testing Performance	Test Results
Diameter	0.75 mm
Length	35 mm
Dimension Ratio	76.08
Volumetric Mass Density	7850 kg/m^3
Ultimate Tensile Strength	400–1200 MPa

2.2. Fabrication of L-Shaped Steel Fibers and Design of Steel Fiber Addition Amounts

The L-shaped steel fibers with a cross-sectional dimension of 17.5 mm × 17.5 mm and a thickness of 0.75 mm were fabricated by manually cold-bending commercial straight steel fibers. The straight steel fibers, type SS-410 stainless steel with a tensile

strength ≥ 1100 MPa and smooth surface, were fixed at one end using a manual fixture during the bending process. Gradual external force was applied to the midpoint of each fiber to cold-bend it into a 90° angle. The mass dosage of steel fibers was designed at 0%, 1%, 2%, and 3%, respectively. The L-shaped fibers are manually bent from straight fibers. The appearance of the fibers is shown in Figure 1.



(**a**) (**b**)

Figure 1. (**a**) Straight steel fiber; (**b**) L-shaped steel fiber.

2.3. Gradation Design of Asphalt Mixture

The gradation design of the asphalt mixture is shown in Table 6.

Table 6. Particle size gradation design for AC-13 asphalt mixture.

Sieve Opening Size (mm)	Composite Gradation (%)
16	100
13.2	93.5
9.5	74.3
4.75	49.3
2.36	30.3
1.18	20.2
0.6	14.2
0.3	9.8
0.15	7.8
0.075	5.1

3. Experimental Items and Test Methods

To elucidate the effects of L-shaped steel fibers on the AC-13 asphalt mixture's mechanical properties, this study delves into their interactions. The following tests were designed: Marshall stability test, high-temperature wheel tracking test, low-temperature small beam bending test, immersion Marshall test, and uniaxial compression test (cylindrical specimen method). All tests were conducted according to the standards specified in *Test Methods for Bitumen and Bituminous Mixtures for Highway Engineering (JTG E20-2011)* [31].

3.1. Marshall Stability and Its Test Method

Marshall stability refers to the maximum load-bearing capacity of asphalt mixture specimens under vertical loading until failure under standard testing conditions. It directly represents the high-temperature compressive resistance of asphalt mixtures and serves as a core indicator for mix design and construction quality control.

In accordance with Test Methods for Bitumen and Bituminous Mixtures for Highway Engineering (JTG E20-2011), standard Marshall specimens (101.6 mm diameter, 63.5 mm

height) were fabricated via the standard compaction method. Subsequently, they were immersed in a 60 °C water bath for 30 min to reach thermal equilibrium. Each test group comprised at least four specimens to ensure statistical reliability. The specimens were loaded at a rate of 50 mm/min using a loading device [31]. The compacted Marshall specimen is shown in Figure 2.



Figure 2. Marshall specimen.

Test data were plotted as load–deformation curves. The deformation at maximum load was recorded as flow value (mm, accurate to 0.1 mm), while the maximum load was measured as stability (kN, accurate to 0.01 kN) using the method shown in Figure 3. The bulk density of Marshall specimens was determined through standard methods, with subsequent calculations of void ratio, mineral aggregate void ratio, and asphalt saturation.

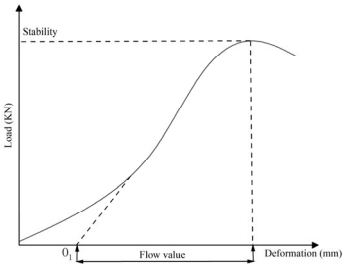


Figure 3. Load–deformation curve.

3.2. Rut Depth, Dynamic Stability and Their Test Methods

In standard rutting tests, rut depth quantifies the permanent deformation of asphalt specimens under cyclic wheel loading. It reflects the actual deformation risk. Dynamic stability is described as the number of wheel-rolling passes required to produce a rut depth of 1 mm within a unit time (usually 45–60 min), which quantifies the rut-resistance performance of materials. Rut depth and dynamic stability are key indices for assessing the high-temperature stability of asphalt mixtures. They directly indicate the pavement's resistance to deformation under high-temperature, heavy-traffic conditions.

In accordance with Test Methods for Bitumen and Bituminous Mixtures for Highway Engineering (JTG E20-2011), rutting tests are conducted to study the dynamic stability of asphalt mixtures with different types and dosages of metal materials added. Plate specimens with dimensions of 300 mm × 300 mm × 50 mm are formed by wheel rolling. The test temperature is set at 60 °C, and the wheel pressure is 0.7 MPa. The specimens are kept at the test temperature for 5 h before the test [31]. The wheel rolling of the rutting test piece is shown in Figure 4.



Figure 4. Wheel rolling of rutting specimens.

The recorder records the rutting deformations d_1 and d_2 at 45 min (t_1) and 60 min (t_2). The calculation method of the dynamic stability is shown in Equation (1) [30].

$$DS = \frac{\left(t_2 - t_1\right) \times N}{d_2 - d_1} \times C_1 \times C_2. \quad (1)$$

In the formula,

DS—the dynamic stability of the asphalt mixture (times/mm);

d_l—the deformation corresponding to the time t_1 (mm);

d_2—the deformation corresponding to the time t_1 (mm);

C_1—the type coefficient of the testing machine, for the operation mode in which the loading wheel is driven by a crank-link mechanism to move back and forth, the coefficient value is 1.0;

C_2—the specimen coefficient. For specimens with a width of 300 mm prepared in the laboratory, the coefficient value is 1.0;

N—the back-and-forth rolling speed of the test wheel, which is typically 42 times per minute.

3.3. Flexural Tensile Strength, Maximum Flexural Tensile Strain, Flexural Stiffness Modulus and Test Methods

The flexural tensile strength tested is the maximum stress value that a material can resist fracture under bending load. The maximum flexural tensile strain represents the peak tensile deformation a material can endure prior to bending failure. The flexural stiffness modulus, calculated as the ratio of bending stress to strain during the material's elastic phase, offers insights into its stiffness properties. To evaluate the material's ability to resist bending deformation under low-temperature scenarios, the standard low-temperature beam bending test is employed. This test effectively characterizes the material's ductility and deformation-resistance capabilities, providing crucial information about its performance in cold environments.

At the optimal asphalt–aggregate ratio for each group, asphalt mixture rutting specimens sized 300 mm × 300 mm × 50 mm are prepared. Subsequently, a cutting machine is utilized to slice the fabricated rutting specimens into beam specimens, each with dimensions of 250 mm × 30 mm × 35 mm. According to the requirements of Test Methods for Bitumen and Bituminous Mixtures for Highway Engineering (JTG E20-2011). Before the test, the beam specimens are placed in a temperature-humidity test chamber at 10 °C for more than 45 min. During the test, the three-point loading method is adopted. For the test, the test span is set at 200 mm, the test temperature is maintained at 10 °C, and the loading rate is fixed at 50 mm/min [31]. The loading process of the beam specimens is shown in Figure 5.

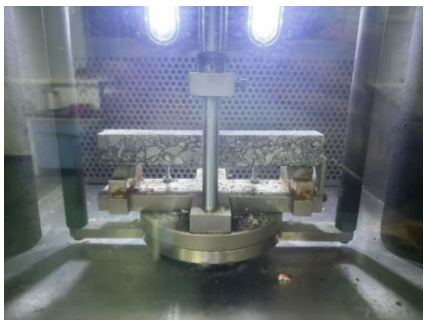


Figure 5. Loading of the beam specimens.

When the specimen fails, the flexural tensile strength R_B, the maximum tensile strain ε_B, and the flexural stiffness modulus S_B of the specimen are calculated according to Equations (2)–(4) [30] as follows:

$$R_B = \frac{3 \times L \times P_B}{2 \times b \times h^2}. \quad (2)$$

$$\varepsilon_{\boldsymbol{B}} = \frac{6 \times h \times d}{L^2}. \quad (3)$$

$$S_{\boldsymbol{B}} = \frac{R_B}{\varepsilon_B}. \quad (4)$$

In the formula,
R_B—the flexural tensile strength when the specimen fails (MPa);
ε_B—the maximum flexural tensile strain when the specimen fails (με);
S_B—the flexural stiffness modulus when the specimen fails (MPa);
b—the width of the specimen at the mid-span cross-section (mm);
h—the height of the specimen at the mid-span cross-section (mm);
L—the span of the specimen (mm);
P_B—the maximum load at which the specimen fails (N);
d—the mid-span deflection when the specimen fails (mm).

3.4. Immersion Marshall Stability, Immersion Residual Stability and Their Test Methods

The immersion Marshall stability refers to the maximum failure load measured through the Marshall test after the asphalt mixture specimen is immersed in water at a specified temperature for a certain period. This indicator is pivotal in assessing the water damage susceptibility of asphalt mixtures. Its value significantly influences the lifespan of pavements in wet environments.

According to Test Methods for Bitumen and Bituminous Mixtures for Highway Engineering (JTG E20-2011). The Marshall specimens are divided into two groups. One group of specimens is immersed in a water bath maintained at a constant temperature of 60 °C for 30 min, after which its Marshall stability is measured. The other group is placed in a 60 °C water bath for 48 h prior to the measurement of its Marshall stability. The water stability of the mixture is characterized by the ratio of the stabilities of these two groups of specimens, namely the immersion residual stability [31]. The partial instruments for the immersion Marshall test are shown in Figures 6 and 7.



Figure 6. Loading of Marshall specimens.



Figure 7. Thermostatic incubator.

The immersion residual stability MS_0 of the specimen is calculated according to Equation (5) [30] as follows:

$$MS_0 = \frac{MS_1}{MS} \times 100. \quad (5)$$

In the formula,
MS_0—the immersion residual stability of the specimen;
MS_1—the stability of the specimen after being immersed in water for 48 h;
MS—the stability of the specimen.

3.5. Freeze–Thaw Splitting Strength, Freeze–Thaw Splitting Strength Ratio and Test Methods

The freeze–thaw splitting strength refers to the maximum failure stress measured in the splitting test after the asphalt mixture specimen has undergone freeze–thaw cycles. It reflects the material's capacity to withstand cracking and resist strength decrease under repeated freeze–thaw effects. The ratio of the splitting strength of a specimen after undergoing freeze–thaw cycles to that of the same specimen without freeze–thaw treatment is defined as the freeze–thaw splitting strength ratio. This ratio serves as a vital metric for assessing the vulnerability of asphalt mixtures to low-temperature water damage.

According to Test Methods for Bitumen and Bituminous Mixtures for Highway Engineering (JTG E20-2011), randomly divide the prepared standard Marshall specimens into two groups (each group containing at least 4 specimens), and measure their diameters and heights. The first group should be stored at room temperature for later use. The second group shall be maintained under a vacuum condition of 97.3–98.7 MPa for 15 min, then immersed in water at normal atmospheric pressure for half an hour. Upon removal, put the specimens into plastic bags. Add 10 mL of water to each bag, seal them tightly, and then store the bags in a constant-temperature freezer set at a temperature of (-18 ± 2) °C for (16 ± 1) h. Subsequently, after retrieving the specimens from the freezer, remove them from the plastic bags and immerse them in a 60 ± 0.5 °C constant-temperature water bath for 24 h. Both groups of specimens are then completely immersed in a 25 ± 0.5 °C constant-

temperature water bath for at least 2 h (with specimen spacing greater than 10 mm). Finally, conduct splitting tests at room temperature (25 °C) using a loading rate of 50 mm/min [31]. Loading of test specimens is shown in Figure 8.

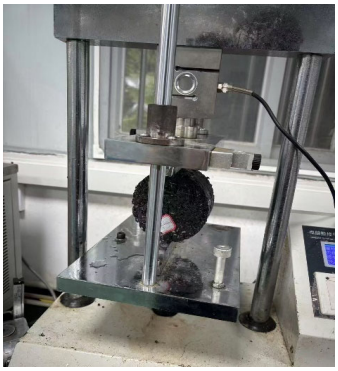


Figure 8. Loading of test specimens.

The freeze–thaw splitting strength ratio is calculated according to Equation (6) [30] as follows:

$$\mathrm{TSR} = \frac{\mathrm{R_{T2}}}{R_{\mathrm{T1}}} \times 100. \quad (6)$$

In the formula,
TSR—freeze–thaw splitting strength ratio (%);
$\mathrm{R_{T1}}$—the average value of the splitting tensile strength of the effective specimens in the first group without freeze–thaw cycles (MPa);
R_{T2}—the average value of the splitting tensile strength of the effective specimens in the second group after freeze–thaw cycles (MPa).

3.6. Compressive Strength, Ultimate Load and Their Test Methods

In the compression test of asphalt mixtures, the compressive strength and ultimate load are measured when the specimens are loaded until they are damaged. The compressive strength reveals the compression resistance of the material per unit area, and it plays a dominant role in the high-temperature stability and structural strength. The ultimate load reflects the overall bearing potential, which is comprehensively affected by factors such as the material composition, construction quality, and stress state. Combined, these two metrics can comprehensively assess the performance of asphalt mixtures in diverse environments, particularly under high-temperature and heavy-load conditions.

Asphalt mixture specimens for the test are formed according to the static pressure method T0704 in Test Methods for Bitumen and Bituminous Mixtures for Highway Engineering (JTG E20-2011). The specimens are 100 mm diameter and 100 mm high cylinders. After forming, the asphalt mixture specimens are placed in a 20 °C constant-temperature water tank for at least 2.5 h, then promptly transferred to the incubator of a universal testing machine to initiate the test. The diameter of the indenter should be larger than that of the specimen itself to ensure that no confining pressure is generated on the specimen when the indenter applies a load to it. The uniaxial compression test is conducted at a loading speed of 50 mm/min. Each test group comprises four asphalt specimens with identical gradations [31]. Uniaxial compression is shown in Figure 9.



Figure 9. Uniaxial compression.

The compressive strength of the specimen is calculated according to Equation (7) [30] as follows:

$$R_c = \frac{4P}{\pi d^2}. \quad (7)$$

In the formula,
R_c—the compressive strength of the specimen (MPa);
P—the maximum load when the specimen fails (N);
d—the diameter of the specimen (mm).

4. Result Analysis

4.1. Results of the Marshall Stability Test

The Marshall stability test was conducted to measure the bulk specific gravity of asphalt mixtures with L-shaped steel fibers and straight steel fibers at dosages of 0%, 1%, 2%, and 3%. Void ratio, voids in mineral aggregate (VMA), asphalt saturation, stability, and flow value were calculated. Four specimens were prepared for each group, and the mean values are shown in Tables 7 and 8.

Table 7. Marshall test results of steel fiber-reinforced asphalt mixture (1).

Type	Dosage/%	Asphalt–Aggregate Ratio/%	Bulk Specific Gravity/g-cm^{-3}	Void Ratio/%
Ordinary Asphalt	0	4.9	4.176	3.94
Straight Steel Fiber	1	4.9	4.208	3.83
	2	4.9	4.211	3.72
	3	4.9	4.231	3.68
L-shaped Steel Fiber	1	4.9	4.205	3.88
	2	4.9	4.216	3.76
	3	4.9	4.235	3.73

Table 8. Marshall test results of steel fiber-reinforced asphalt mixture (2).

Type	Dosage/%	Voids in Mineral Aggregate/%	Asphalt Saturation/%	Stability/KN	Flow Value/mm
Ordinary Asphalt	0	14.15	71.25	12.13	3.39
Straight Steel Fiber	1	14.12	71.81	13.21	3.51
	2	14.06	72.47	14.02	3.64
	3	13.92	73.05	13.73	3.69
L-shaped Steel Fiber	1	14.08	71.71	13.56	3.55
	2	13.98	72.53	14.31	3.71
	3	13.90	73.22	13.84	3.76

This study conducted a comparative analysis of the Marshall performance between conventional asphalt mixtures and those reinforced with straight or L-shaped steel fibers. All specimens were prepared with an asphalt–aggregate ratio of 4.9%, ensuring a consistent basis for performance evaluation.

According to Technical Specifications for Construction of Highway Asphalt Pavements (JTG F40-2004), the stability requirement is >8 kN, and the change is shown in Figure 10. The void ratio requirement is 3–5%, and all data fell within the specified range, meeting the requirements. The voids in mineral aggregate (VMA) requirement is ≥ 14%, and both the ordinary asphalt and fiber-reinforced mixtures met the minimum value specified in the *specifications*. The asphalt saturation requirement is 65–75%, and the asphalt saturation of the specimens complied with the standard. All data met the code requirements, and the L-shaped steel fiber exhibited the best comprehensive performance at a dosage of 2% [30].

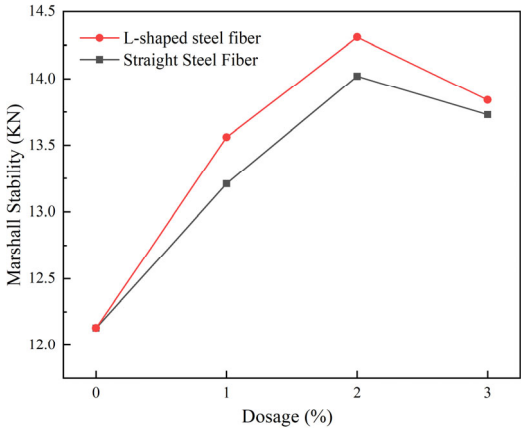


Figure 10. Marshall stability test results.

4.2. Analysis of the Influence of L-Shaped Steel Fibers on the High-Temperature Rutting Resistance of Asphalt Mixtures

Rutting tests were conducted on asphalt mixtures with L-shaped and straight steel fibers at dosages of 0% (control), 1%, 2%, and 3% to measure rut depth and dynamic stability. Four specimens were prepared for each group, and the mean values are shown in Table 9.

Table 9. Rutting test results.

Type	Dosage/%	Rutting Depth/mm 45 min	Rutting Depth/mm 60 min	Dynamic Stability/Times·mm^{-1}	Specification Requirement
Ordinary Asphalt	0	2.083	2.246	3865	Dynamic Stability ≥ 3000
Straight Steel Fiber	1	1.876	2.029	4118	
	2	1.813	1.952	4532	
	3	1.817	1.959	4468	
L-shaped Steel Fiber	1	1.842	1.991	4228	
	2	1.823	1.959	4632	
	3	1.839	1.978	4532	

4.2.1. Analysis of Discreteness and Stability

As shown in Tables 10 and 11, from the dispersibility perspective, the L-shaped steel fiber group exhibited significantly lower coefficients of variation than the straight steel fiber group, with coefficients of variation for rutting depth below 3.5% at 2% and

3% dosages, indicating enhanced uniform distribution and reduced test fluctuations. In contrast, the straight steel fiber group showed the coefficient of variation in rutting depth approaching 10% at high dosages, potentially due to material inhomogeneity from fiber agglomeration or variability in testing loading conditions. All data satisfied strict material testing dispersibility requirements: the L-shaped steel fiber group demonstrated excellent low-variability performance across dosages, while the straight steel fiber group necessitated attention to fiber uniformity at high dosages. Despite these dosage-dependent coefficients of variation differences, the overall experimental results remained reliable within acceptable variability ranges for both fiber types.

Table 10. The standard deviation of rutting depth and dynamic stability.

Standard Deviation				
Type	**Dosage/%**	**Rutting Depth/45 min**	**Rutting Depth/60 min**	**Dynamic Stability**
Ordinary Asphalt	0	0.0737	0.1027	81.2358
Straight Steel Fiber	1	0.0957	0.1155	163.9399
	2	0.0995	0.1369	179.1118
	3	0.1720	0.1653	229.2627
L-shaped Steel Fiber	1	0.0909	0.0784	170.1930
	2	0.0528	0.0577	126.2900
	3	0.0628	0.0306	103.7764

Table 11. The coefficient of variation of rutting depth and dynamic stability.

Coefficient of Variation				
Type	**Dosage/%**	**Rutting Depth/45 min**	**Rutting Depth/60 min**	**Dynamic Stability**
Ordinary Asphalt	0	3.54%	4.57%	2.10%
Straight Steel Fiber	1	5.10%	5.69%	3.98%
	2	5.49%	7.01%	3.95%
	3	9.47%	8.44%	5.13%
L-shaped Steel Fiber	1	4.93%	2.43%	4.02%
	2	2.90%	1.41%	2.73%
	3	3.41%	1.55%	2.29%

4.2.2. Comparison of Rutting Resistance Between L-Shaped Steel Fiber-Reinforced Asphalt Mixtures and Straight Steel Fiber-Reinforced Asphalt Mixtures

As can be seen from Figures 11 and 12, with the addition of steel fibers, at 45 min, the rut depth decreases to 1.823 mm when the dosage is 2%, which is 12.5% lower than that of ordinary asphalt. At 60 min, the rut depth decreases to 1.959 mm when the dosage is 2%, which is 12.8% lower than that of ordinary asphalt. Meanwhile, the dynamic stability of the L-shaped steel fiber-reinforced asphalt mixture reaches 4632 times/mm when the dosage is 2%, which is 19.9% higher than that of ordinary asphalt.

At 45 min, the rut depth of the straight steel fiber-reinforced asphalt mixture decreases to 2.083 mm when the dosage is 2%, while the rut depth of the L-shaped steel fiber-reinforced asphalt mixture decreases to 1.823 mm at the same dosage. At 60 min, the rut depth of the straight steel fiber-reinforced asphalt mixture decreases to 2.246 mm when the dosage is 2%, and that of the L-shaped steel fiber-reinforced asphalt mixture decreases to 1.959 mm at a 2% dosage. Meanwhile, the dynamic stability of the L-shaped steel fiber-reinforced asphalt mixture reaches a peak of 4632 times/mm when the fiber dosage is 2%, and its core index is 2.2% higher than that of the straight steel fiber.

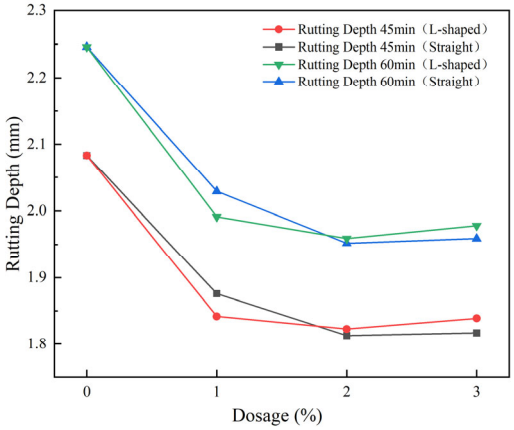


Figure 11. Comparison of rutting depth between L-shaped and straight steel fibers.

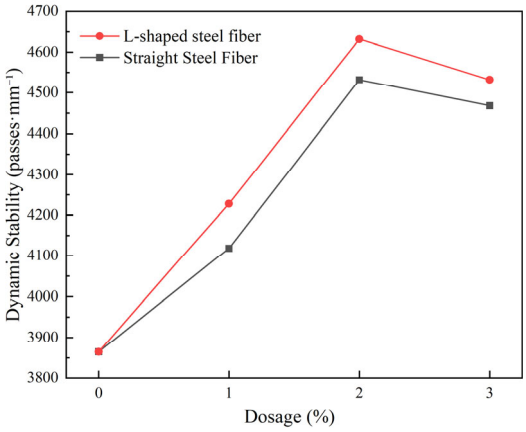


Figure 12. Comparison of dynamic stability between L-shaped and straight steel fibers.

Analysis of the rutting test results reveals that L-shaped steel fibers significantly enhance the high-temperature rutting resistance of the mixture, outperforming straight steel fibers in terms of reinforcement efficiency. This superiority can be attributed to the unique structural characteristics of L-shaped fibers. Upon incorporation, these fibers form a robust skeleton-locking structure within the mixture, interweaving with aggregates to restrict their relative movement at elevated temperatures. The mechanical interlocking and anchoring mechanisms provided by L-shaped fibers directly contribute to an increase in the mixture's overall stiffness. Additionally, the high thermal conductivity of steel fibers promotes a more uniform temperature field distribution, mitigating the risk of localized softening and further enhancing the mixture's rutting resistance.

4.3. Analysis of the Influence of L-Shaped Steel Fibers on the Low-Temperature Crack Resistance of Asphalt Mixtures

Low-temperature beam bending tests were performed on asphalt mixtures with L-shaped and straight steel fibers at dosages of 0%, 1%, 2%, and 3%. The tests measured flexural tensile strength, maximum flexural tensile strain, and flexural modulus. Four specimens were prepared for each group, and the mean values are shown in Table 12.

Table 12. Results of low-temperature beam bending test.

Type	Dosage/%	Flexural Tensile Strength RB (MPa)	Maximum Flexural Tensile Strain εB (με)	Flexural Stiffness Modulus SB (MPa)	Specification Requirement
Ordinary Asphalt	0	9.31	2762	3373	Maximum Flexural Tensile Strain ≥ 2500 με
Straight Steel Fiber	1	10.20	3082	3311	
	2	10.78	3313	3255	
	3	10.62	3245	3273	
L-shaped Steel Fiber	1	10.43	3155	3306	
	2	11.17	3423	3262	
	3	10.87	3297	3298	

4.3.1. Analysis of Discreteness and Stability

As shown in Tables 13 and 14, the coefficients of variation of the indices for the L-shaped steel fiber group are between 2% and 6%, indicating a low degree of dispersion and relatively good stability across different dosages which demonstrates that the L-shaped steel fibers play a positive role in maintaining the stability of the flexural stiffness modulus of the material while for the straight steel fiber group the coefficients of variation of the indices range from 5% to 10% and some of them even exceed 10% indicating that a high dosage of straight steel fibers may lead to inhomogeneity in the internal structure of the material or there are certain factors during the test process that affect the stability of the test results thus increasing the degree of dispersion of the indices but the overall test results are reliable.

Table 13. The standard deviation of flexural tensile, maximum flexural tenstraine strain and flexural stiffness modulus.

Standard Deviation				
Type	**Dosage/%**	**Flexural Tensile Strength RB**	**Maximum Flexural Tensile Strain εB**	**Flexural Stiffness Modulus SB**
Ordinary Asphalt	0	0.3398	37.1179	93.4933
Straight Steel Fiber	1	0.6702	161.4214	176.6974
	2	0.8729	105.2205	154.8879
	3	1.2053	173.6134	283.0499
L-shaped Steel Fiber	1	0.5518	102.4214	123.2136
	2	0.4824	108.6620	90.1300
	3	0.4605	90.2205	70.9143

Table 14. The coefficient of variation of flexural tensile, maximum flexural tenstraine strain and flexural stiffness modulus.

Coefficient of Variation				
Type	**Dosage/%**	**Flexural Tensile Strength RB**	**Maximum Flexural Tensile Strain εB**	**Flexural Stiffness Modulus SB**
Ordinary Asphalt	0	3.65%	1.34%	2.77%
Straight Steel Fiber	1	6.57%	5.24%	5.34%
	2	8.11%	3.18%	4.76%
	3	11.35%	5.35%	8.65%
L-shaped Steel Fiber	1	5.29%	3.25%	3.73%
	2	4.32%	3.17%	2.76%
	3	4.24%	2.73%	2.15%

4.3.2. Comparison of Low-Temperature Crack Resistance Between L-Shaped Steel Fiber-Reinforced Asphalt Mixtures and Straight Steel Fiber-Reinforced Asphalt Mixtures

It can be seen from Figures 13–15, with the addition of steel fibers, the low-temperature crack resistance of the asphalt mixture is remarkably improved. The performance reaches

its peak when the dosage of L-shaped steel fibers is 2%. The flexural tensile strength amounts to 11.17 MPa, registering a 20.0% increment compared to that of ordinary asphalt (9.31 MPa). The maximum flexural tensile strain is 3423 με, representing a 23.9% increase over that of ordinary asphalt (2762 με). The flexural stiffness modulus is 3262 MPa, which is 3.3% lower than that of ordinary asphalt (3373 MPa). This evidently indicates that the addition of L-shaped steel fibers augments the flexibility of the material and confers superior low-temperature adaptability.

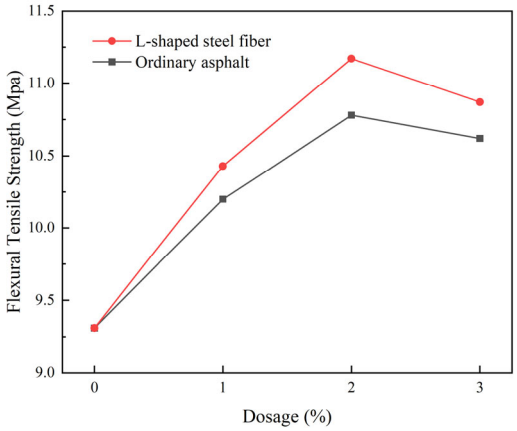


Figure 13. Comparison of flexural tensile strength between L-shaped and straight steel fibers.

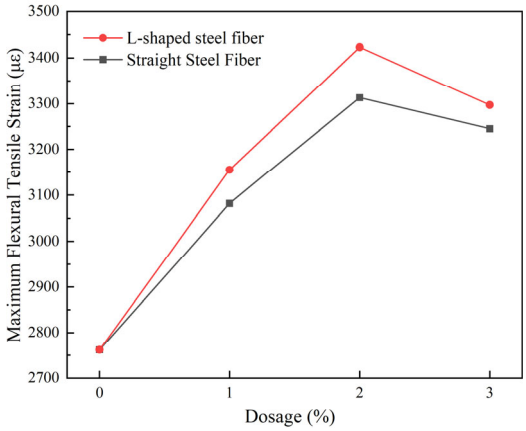


Figure 14. Comparison of maximum tensile strain between L-shaped and straight steel fibers.

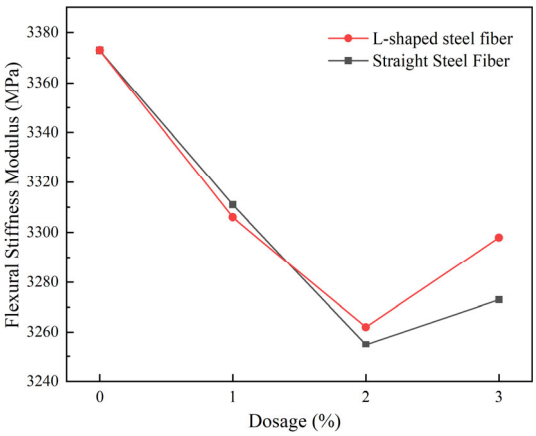


Figure 15. Comparison of flexural stiffness modulus between L-shaped and straight steel fibers.

The flexural tensile strength of L-shaped steel fibers reaches a peak of 11.17 MPa when the dosage is 2%, which is 3.6% higher than that of straight steel fibers (10.78 MPa). The

maximum flexural tensile strain of L-shaped steel fibers reaches a peak of 3423 με when the dosage is 2%, which is 3.3% higher than that of straight steel fibers (3313 με). The flexural stiffness modulus of L-shaped steel fibers reaches a peak of 3262 MPa when the dosage is 2%, which is slightly higher than that of straight steel fibers (3255 MPa), indicating better flexibility. When the dosage is 3%, the performance relatively declines, but the reinforcement effect of L-shaped steel fibers is still better than that of straight steel fibers.

Based on comprehensive analysis, in a low-temperature environment, if the modulus is too high, the elastic stiffness is higher, and the material is too brittle and prone to cracking; when the modulus is moderate, the flexibility of the mixture is better. With the addition of L-shaped steel fibers and straight steel fibers, the flexural stiffness modulus measured in the test decreases.

4.4. Analysis of the Influence of L-Shaped Steel Fibers on the Water Damage Resistance of Asphalt Mixtures

Marshall tests were conducted on asphalt mixtures containing L-shaped and straight steel fibers at dosages of 0%, 1%, 2%, and 3%. The tests measured immersion Marshall stability, residual immersion stability, and Marshall stability. Four specimens were prepared for each group, and the mean values are shown in Table 15.

Table 15. Results of immersion Marshall test.

Type	Dosage/%	Marshall Stability/KN	Immersion Marshall Stability/KN	Immersion Residual Stability/%	Specification Requirement
Ordinary Asphalt	0	12.31	11.06	89.84	Immersion Residual Stability ≥ 85%
Straight Steel Fiber	1	13.42	12.39	92.32	
	2	14.39	13.51	93.88	
	3	13.61	12.59	92.51	
L-shaped Steel Fiber	1	13.51	12.47	92.30	
	2	14.76	13.88	94.04	
	3	14.36	13.32	92.76	

4.4.1. Analysis of Discreteness and Stability

As shown in Tables 16 and 17, the coefficients of variation of the indices for the L-shaped steel fiber group range from 2% to 6%, and the coefficients of variation in Marshall stability before and after immersion are generally lower than those of the straight steel fiber group, indicating high performance stability of the material under immersion conditions, while the coefficients of variation of the indices for the straight steel fiber group range from 4% to 8%, suggesting that the addition of straight steel fibers increases the dispersion degree of the material's immersion Marshall stability, possibly associated with the influence of steel fibers on asphalt under immersion conditions and the changes in the internal structure of the material.

Table 16. The standard deviation of Marshall stability and immersion Marshall stability.

Standard Deviation			
Type	**Dosage/%**	**Marshall Stability**	**Immersion Marshall Stability**
Ordinary Asphalt	0	0.3106	0.4772
Straight Steel Fiber	1	0.6568	0.7542
	2	0.7105	0.9654
	3	0.9348	0.9253
L-shaped Steel Fiber	1	0.6525	0.5852
	2	0.6348	0.4995
	3	0.4995	0.6260

Table 17. The coefficient of variation of Marshall stability and immersion Marshall stability.

Coefficient of Variation			
Type	**Dosage/%**	**Marshall Stability**	**Immersion Marshall Stability**
Ordinary Asphalt	0	2.52%	4.31%
Straight Steel Fiber	1	4.89%	6.10%
	2	4.93%	7.15%
	3	6.87%	7.35%
L-shaped Steel Fiber	1	4.83%	4.70%
	2	4.30%	3.60%
	3	3.48%	4.70%

4.4.2. Comparison of Water Damage Resistance Between L-Shaped Steel Fiber Reinforced Asphalt Mixtures and Straight Steel Fiber-Reinforced Asphalt Mixtures

It can be seen from Figures 16 and 17, with the addition of L-shaped steel fibers, the Marshall stability of the asphalt mixture is gradually enhanced. The Marshall stability reaches a maximum of 14.76 kN when the dosage is 2%, which is 19.9% higher than that of ordinary asphalt (12.31 kN). Through a calculation and analysis of the Marshall stability after immersion, the peak value of the residual immersion stability calculated for L-shaped steel fibers is 94.04%. Compared with the residual immersion stability of ordinary asphalt (89.84%), it has increased by 4.2 percentage points. When the dosage is 3%, the residual immersion stability relatively decreases but still remains at 92.76%, which is still better than that of ordinary asphalt.

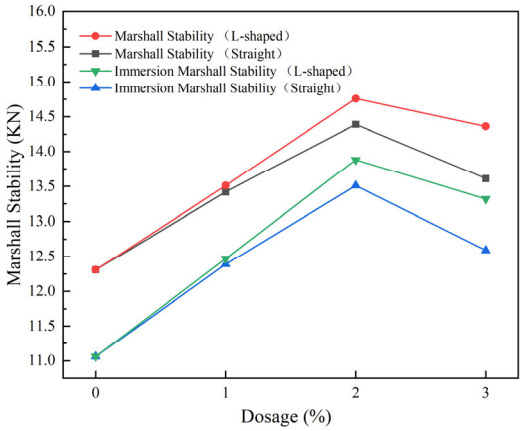


Figure 16. Comparison of Marshall stability between L-shaped and straight steel fibers.

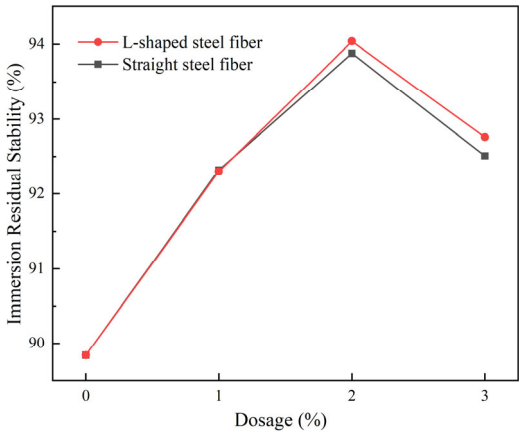


Figure 17. Comparison of immersion Marshall stability between L-shaped and straight steel fibers.

At the optimal dosage of 2%, L-shaped fibers form a denser three-dimensional reinforcement network through the end-hook anchorage effect. The residual immersion stability reaches 94.04%, which is 0.16% higher than that of straight steel fibers (93.88%). When the dosage is excessive at 3%, L-shaped fibers inhibit agglomeration by virtue of their geometric self-locking characteristics, and the residual immersion stability remains at 92.76%, which is still 0.25 percentage points better than that of straight steel fibers (92.51%). In terms of the residual immersion stability, both straight and L-shaped steel fibers effectively enhance the water damage resistance of asphalt mixtures. Although the performance improvement of L-shaped fibers is marginally better, the difference between the two fiber types remains negligible. This proves that its unique geometric design can more effectively block the water penetration path and enhance the durability of interface bonding. Especially under the long-term water-force coupling effect, the performance degradation is slower.

4.5. Analysis of the Influence of L-Shaped Steel Fibers on the Freeze–Thaw Splitting Strength of Asphalt Mixtures

Freeze–thaw splitting tests were conducted on asphalt mixtures with L-shaped and straight steel fibers at dosages of 0%, 1%, 2%, and 3%. Four specimens were prepared for each group, and the mean values are shown in Table 18.

Table 18. Results of freeze–thaw splitting test.

Type	Dosage/%	Unfrozen–Thawed Splitting Strength Rt1/MPa	Post-Freeze–Thawed Splitting Strength Rt2/MPa	Freeze–Thaw Splitting Strength Ratio/%	Specification Requirement
Ordinary Asphalt	0	1.08	0.89	82.56	Freeze–thaw Splitting Strength Ratio ≥ 80%
Straight Steel Fiber	1	1.16	0.98	84.48	
	2	1.19	1.01	85.01	
	3	1.18	1.00	84.60	
L-shaped Steel Fiber	1	1.23	1.04	84.75	
	2	1.37	1.17	85.14	
	3	1.26	1.07	84.99	

4.5.1. Analysis of Discreteness and Stability

As shown in Tables 19 and 20, the coefficients of variation of the indices for the L-shaped steel fiber group range from 4% to 10%. The coefficients of variation in the splitting

strength both before and after freeze–thaw are generally lower than those of the straight steel fiber group and are not significantly different from those of ordinary asphalt. The coefficients of variation of the indices for the straight steel fiber group range from 8% to 15%. The addition of straight steel fibers causes significant fluctuations in the dispersion degree of the material's splitting strength after freeze–thaw, which may be related to the effect of steel fibers on asphalt during the freeze–thaw cycle and the changes in the internal structure of the material.

Table 19. The standard deviation of unfrozen–thawed splitting strength and post-freeze–thawed splitting strength.

Standard Deviation			
Type	**Dosage/%**	**Unfrozen–Thawed Splitting Strength Rt1**	**Post-Freeze–Thawed Splitting Strength Rt2**
Ordinary Asphalt	0	0.0426	0.0852
Straight Steel Fiber	1	0.0932	0.1245
	2	0.1203	0.0912
	3	0.1348	0.1446
L-shaped Steel Fiber	1	0.0821	0.0965
	2	0.0675	0.0522
	3	0.0590	0.0675

Table 20. The coefficient of variation of unfrozen–thawed splitting strength and post-freeze–thawed splitting strength.

Coefficient of Variation			
Type	**Dosage/%**	**Unfrozen–Thawed Splitting Strength Rt1**	**Post-Freeze–Thawed Splitting Strength Rt2**
Ordinary Asphalt	0	3.94%	9.57%
Straight Steel Fiber	1	8.03%	12.70%
	2	10.11%	9.03%
	3	11.42%	14.46%
L-shaped Steel Fiber	1	6.68%	9.28%
	2	4.93%	4.46%
	3	4.68%	6.31%

4.5.2. Comparison of Freeze–Thaw Splitting Resistance Between L-Shaped Steel Fiber-Reinforced Asphalt Mixtures and Straight Steel Fiber-Reinforced Asphalt Mixtures

It can be seen from Figures 18 and 19 that, in the absence of freeze–thaw cycles, the splitting resistance of asphalt mixtures steadily improves with the incorporation of L-shaped steel fibers. The splitting strength peaks at 1.37 MPa with a 2% fiber dosage, representing a 26.85% increase compared to plain asphalt. After freeze–thaw treatment, the specimens achieve a maximum splitting strength of 1.17 MPa at the same 2% dosage, a 31.46% enhancement over the control group. Additionally, the freeze–thaw splitting strength ratio increases by 2.58%, confirming the effectiveness of L-shaped steel fibers in enhancing freeze–thaw resistance. Throughout the fiber addition process, L-shaped fibers consistently improve asphalt mixture performance, both before and after freeze–thaw. Although a slight performance decline occurs at a 3% dosage, the fibers' positive impact on freeze–thaw resistance remains significant.

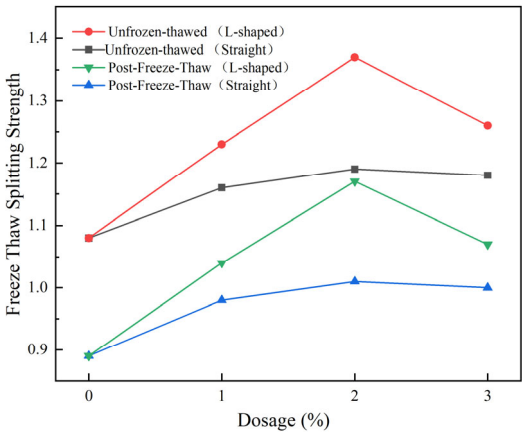


Figure 18. Comparison of freeze–thaw splitting strength between L-shaped and straight steel fibers.

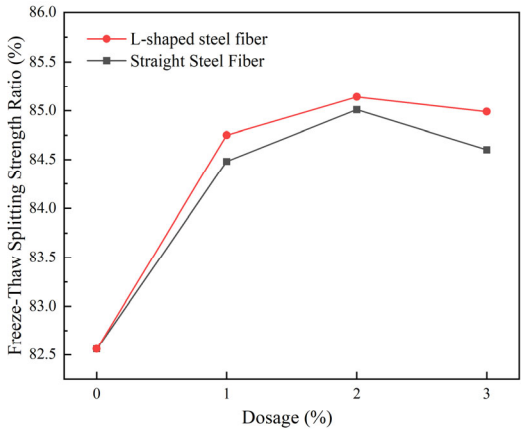


Figure 19. Comparison of freeze–thaw splitting strength ratio between L-shaped and straight steel fibers.

Without freeze–thaw treatment, the splitting strength of straight steel fiber-reinforced asphalt mixture peaks at 1.19 MPa, whereas that of L-shaped steel fiber-reinforced asphalt mixture reaches 1.37 MPa at the same dosage. After freeze–thaw, the maximum splitting strength of straight and L-shaped steel fiber-reinforced mixtures is 1.01 MPa and 1.17 MPa, respectively. The freeze–thaw splitting strength ratio of the L-shaped steel fiber-reinforced mixture is 85.14%, 0.13 percentage points higher than that of the straight steel fiber-reinforced mixture (85.01%).

Based on the above comparative analysis of splitting strength results, it can be seen that L-shaped steel fibers significantly enhance the freeze–thaw resistance of asphalt mixtures, and there is not much difference between them and straight steel fibers. L-shaped steel fibers can reduce interface delamination during freeze–thaw cycles, inhibit water intrusion and ice crystal expansion damage, disperse freeze–thaw stress through the formed fiber network, and reduce the probability of micro-crack initiation.

4.6. Analysis of the Influence of L-Shaped Steel Fibers on the Compressive Performance of Asphalt Mixtures

The uniaxial compression test was carried out to measure the ultimate load and compressive strength of asphalt mixtures with L-shaped steel fiber and straight steel fiber dosages of 0%, 1%, 2% and 3%. Four specimens were prepared for each group, and the mean values are shown in Table 21.

Table 21. Results of uniaxial compression test.

Type	Dosage/%	Ultimate Load/KN	Compressive Strength/MPa
Ordinary Asphalt	0	40.13	5.11
Straight Steel Fiber	1	43.32	5.52
	2	46.15	5.88
	3	45.43	5.79
L-shaped Steel Fiber	1	44.63	5.68
	2	47.26	6.02
	3	46.22	5.89

4.6.1. Standard Deviation and Coefficient of Variation

As shown in Tables 22 and 23, for the L-shaped steel fiber group, increasing the dosage from 1% to 3% reduced the coefficient of variation of the ultimate load from 5.65% to 2.94% and the coefficient of variation of the compressive strength from 5.46% to 3.13%. This decline in coefficients of variation indicates improved material uniformity and enhanced performance stability with higher fiber content.

Table 22. The standard deviation of ultimate load and compressive strength.

Standard Deviation			
Type	**Dosage/%**	**Ultimate Load**	**Compressive Strength**
Ordinary Asphalt	0	2.0082	0.2618
Straight Steel Fiber	1	3.1906	0.3238
	2	2.4314	0.3638
	3	4.2082	0.3638
L-shaped Steel Fiber	1	2.5201	0.3103
	2	1.6574	0.2450
	3	1.3586	0.1845

Table 23. The coefficient of variation of ultimate Load and compressive strength.

Coefficient of Variation			
Type	**Dosage/%**	**Ultimate Load**	**Compressive Strength**
Ordinary Asphalt	0	5.00%	5.12%
Straight Steel Fiber	1	7.37%	5.87%
	2	5.27%	6.19%
	3	9.26%	6.28%
L-shaped Steel Fiber	1	5.65%	5.46%
	2	3.51%	4.07%
	3	2.94%	3.13%

In contrast, the straight steel fiber group showed pronounced fluctuations in coefficients of variation across dosages. The coefficients of variation of the ultimate load ranged from 5.27% to 9.26%, and those of the compressive strength varied between 5.87% and 6.28%, with the former showing greater variability. This suggests that straight steel fiber dosages significantly impact the dispersion of the ultimate load property.

Overall, the L-shaped steel fiber group exhibited lower coefficients of variation than the straight steel fiber group, especially at higher dosages, demonstrating its superior control over material property dispersion.

4.6.2. Comparison of Compressive Performance Between L-Shaped Steel Fiber-Reinforced Asphalt Mixtures and Straight Steel Fiber-Reinforced Asphalt Mixtures

As illustrated in Figures 20 and 21, incorporating L-shaped steel fibers significantly enhances the compressive performance of asphalt mixtures. At a 2% fiber dosage, the ultimate load peaks at 47.26 kN, corresponding to a maximum compressive strength of 6.02 MPa—an increase of 17.8% compared to plain asphalt. As the dosage of L-shaped steel fibers increases, the compressive strength initially rises, reaches a maximum, and then begins to decline. Nevertheless, the overall improvement in the compressive strength of the asphalt mixtures remains substantial.

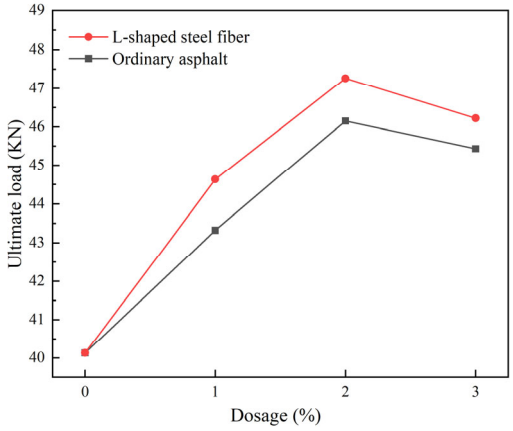


Figure 20. Comparison of ultimate load between L-shaped and straight steel fibers.

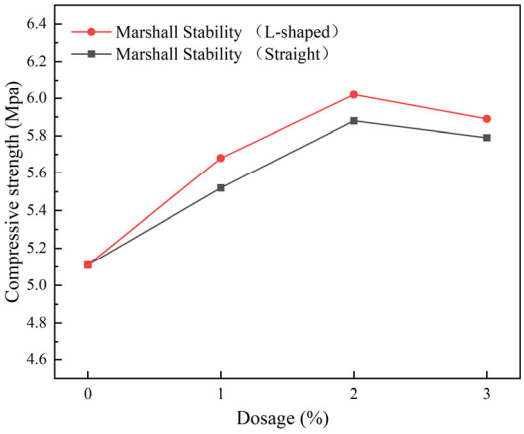


Figure 21. Comparison of compressive strength between L-shaped and straight steel fibers.

An analysis of the ultimate load and compressive strength of L-shaped and straight steel fibers at different dosages reveals the following trends. The compressive strength of straight steel fibers rises initially and subsequently declines as the dosage increases, peaking at 5.88 MPa when the dosage reaches 2%. Similarly, the compressive strength of L-shaped steel fibers follows an increasing-then-decreasing pattern with dosage increments, attaining a maximum of 6.02 MPa at a 2% dosage. Moreover, the ultimate load of L-shaped fibers (47.26 kN) exceeds that of straight steel fibers (46.15 kN), aligning with the upward trend in compressive strength values. The addition of L-shaped steel fibers can significantly enhance the compressive strength of the asphalt mixture, and it is slightly better than that of straight steel fibers in terms of reinforcement effect. Both types of steel fibers reach their peak values when the dosage is 2%. The compressive strength of L-shaped steel fibers is 0.14 MPa higher than that of straight steel fibers, with a higher increase range. However,

when an excessive amount of either type of fiber is added, the performance may slightly decline due to uneven fiber distribution or deterioration of interfacial bond performance.

5. Conclusions

In the field of road engineering, the research on the influence of L-shaped steel fibers on the performance of asphalt mixtures is of great significance. Experimental results indicate that L-shaped steel fibers exhibit multifaceted reinforcing characteristics, thereby enhancing the overall performance of asphalt mixtures by approximately 20%. Their reinforcing performance is slightly superior to that of straight steel fibers. By quantifying data dispersion through standard deviation and coefficient of variation, L-shaped steel fibers exhibit smaller values for both indices, demonstrating that their reinforcing effect on asphalt mixtures is less variable, more uniform, and more stable. As a result, the following conclusions can be drawn:

(1) High-temperature rutting resistance

With respect to high-temperature rutting resistance, the rut depth of asphalt mixtures incorporating L-shaped steel fibers decreases by 12%. The core parameter—dynamic stability—exhibits a 2.2% improvement compared to straight steel fiber-reinforced asphalt mixtures. Although the numerical difference is modest, the L-shaped steel fiber group had notably lower coefficients of variation than the straight steel fiber group. At 2% and 3% dosages, the coefficients of variation for rutting depth were below 3.5%, suggesting better uniformity and less test variability.

(2) Low-temperature crack resistance

In terms of low-temperature crack resistance, the reinforcing effect of L-shaped steel fibers on asphalt mixtures increases by approximately 20%. At the optimal steel fiber dosage, L-shaped steel fiber-reinforced asphalt mixtures show a 3.6% enhancement over straight steel fiber-reinforced counterparts. The coefficients of variation of various indices for the L-shaped steel fiber group range from 2% to 6%. Compared with those of the straight steel fiber group, which range from 5% to 10%, the L-shaped steel fiber group exhibits better stability.

(3) Water damage resistance

For water damage resistance, the Marshall stability of L-shaped steel fiber-reinforced mixtures increases by 19.9% relative to ordinary asphalt mixtures. The residual immersion stability of straight steel fiber-reinforced asphalt mixtures is 93.88%, whereas that of L-shaped steel fiber-reinforced mixtures reaches 94.04%, representing a 0.16 percentage point increase. The L-shaped steel fiber group exhibits coefficient of variation values between 2% and 6% for all indices, compared to 4–8% for the straight steel fiber group. Notably, its Marshall stability coefficients of variation before and after immersion are consistently lower than those of the straight steel fiber group.

(4) Freeze–thaw splitting strength

Regarding freeze–thaw splitting strength, L-shaped steel fibers increase the pre-freeze–thaw splitting strength of asphalt mixtures by 26% and post-freeze–thaw splitting strength by up to 30%. The freeze–thaw splitting strength ratio of straight steel fiber-reinforced mixtures is 85.01%, compared to 85.14% for L-shaped steel fiber-reinforced mixtures—a 0.13 percentage point increase. The coefficients of variation of various indices for the L-shaped steel fiber group range from 4% to 10%, showing relatively good stability. In contrast, the coefficients of variation of the indices for the straight steel fiber group range from 8% to 15%, indicating greater volatility.

(5) Compressive strength

In the context of compressive strength, L-shaped steel fibers increase the ultimate load of asphalt mixtures by 17%. The compressive strength of straight steel fiber-reinforced mixtures is 5.88 MPa, whereas that of L-shaped steel fiber-reinforced mixtures is 6.02 MPa, reflecting a 2.4% increase. As the dosage of the L-shaped steel fiber group increases, the coefficients of variation in both the ultimate load and the compressive strength decrease. In contrast, for the straight steel fiber group, the situation is the opposite, indicating that its dosage significantly affects the dispersion of the ultimate load.

Collectively, L-shaped steel fibers exhibit superior reinforcing effects on asphalt mixtures. Compared to straight fibers, their unique geometric configuration provides a marginal improvement in the mechanical properties of the mixture, accompanied by a more uniform and stable enhancement. Future studies should focus on optimizing steel fiber parameters and validating the material's applicability and reliability in real-world engineering scenarios.

Author Contributions: Conceptualization, Q.Y. and W.Y.; methodology, Q.Y., W.Y. and J.C.; validation Q.Y., W.Y. and Y.L. (Ya Li); investigation, Y.Z., K.C. and Y.L. (Ya Li); writing—original draft, Q.Y.; writing—review and editing, W.Y. and Y.L (Yunhao Li). All authors have read and agreed to the published version of the manuscript.

Funding: This research received no external funding.

Data Availability Statement: All the data are present within the article.

Acknowledgments: The first two authors would like to thank the department of civil engineering at Chongqing Jiaotong University for partially supporting this work.

Conflicts of Interest: The authors declare no conflicts of interest.

References

1. Hu, J.; Liu, P.; Wang, D.; Oeser, M.; Tan, Y. Investigation on Fatigue Damage of Asphalt Mixture with Different Air-Voids Using Microstructural Analysis. *Constr. Build. Mater.* **2016**, *125*, 936–945. [CrossRef]
2. Zheng, C.; Xu, J.; Zhang, T.; Tan, G. Study on the Microscopic Damage of Porous Asphalt Mixture under the Combined Action of Hydrodynamic Pressure and Ice Crystal Frost Heave. *Constr. Build. Mater.* **2021**, *303*, 124489. [CrossRef]
3. Qin, X.; Shen, A.; Guo, Y.; Li, Z.; Lv, Z. Characterization of Asphalt Mastics Reinforced with Basalt Fibers. *Constr. Build. Mater.* **2018**, *159*, 508–516. [CrossRef]
4. Wu, B.; Pei, Z.; Luo, C.; Xia, J.; Chen, C.; Kang, A. Effect of Different Basalt Fibers on the Rheological Behavior of Asphalt Mastic. *Constr. Build. Mater.* **2022**, *318*, 125718. [CrossRef]
5. Piuzzi, G.P.; Scheuermann Filho, H.C.; Villena Del Carpio, J.A.; Consoli, N.C. The Effects of Porosity, Asphalt Content and Fiberglass Incorporation on the Tensile Strength and Resilient Modulus of Asphalt Concrete Blends. *Geotext. Geomembr.* **2021**, *49*, 864–870. [CrossRef]
6. Yang, Q.; Hong, B.; Lin, J.; Wang, D.; Zhong, J.; Oeser, M. Study on the Reinforcement Effect and the Underlying Mechanisms of a Bitumen Reinforced with Recycled Glass Fiber Chips. *J. Clean. Prod.* **2020**, *251*, 119768. [CrossRef]
7. Pirmohammad, S.; Majd Shokorlou, Y.; Amani, B. Influence of Natural Fibers (Kenaf and Goat Wool) on Mixed Mode I/II Fracture Strength of Asphalt Mixtures. *Constr. Build. Mater.* **2020**, *239*, 117850. [CrossRef]
8. Pirmohammad, S.; Hojjati Mengharpey, M. Influence of Natural Fibers on Fracture Strength of WMA (Warm Mix Asphalt) Concretes Using a New Fracture Test Specimen. *Constr. Build. Mater.* **2020**, *251*, 118927. [CrossRef]
9. Wang, S.; Mallick, R.B.; Rahbar, N. Toughening Mechanisms in Polypropylene Fiber-Reinforced Asphalt Mastic at Low Temperature. *Constr. Build. Mater.* **2020**, *248*, 118690. [CrossRef]
10. Mohd Rodzi, A.S.; Masri, K.A.; Shahnewaz, S.M.; Ferdaus, R.; Abd Ghani, N.A.A.; Arshad, A.K. Microstructure Analysis and Permanent Deformation of Porous Asphalt Incorporating Steel Fiber. *IOP Conf. Ser. Earth Environ. Sci.* **2024**, *1296*, 012018. [CrossRef]
11. Nian, T.; Wang, M.; Ge, J.; Guo, R.; Li, P.; Song, J. Enhancing Low-Temperature Crack Resistance: A Method for Establishing Meso-Models and Evaluating Steel Fiber-Reinforced Hot Recycled Asphalt Mixtures. *Constr. Build. Mater.* **2024**, *438*, 137026. [CrossRef]
12. Fu, L.; Jiao, Y.; Chen, X. Reinforcement Evaluation of Different Fibers on Fracture Resistance of Asphalt Mixture Based on Acoustic Emission Technique. *Constr. Build. Mater.* **2022**, *314*, 125606. [CrossRef]

13. Yang, H.; Ouyang, J.; Jiang, Z.; Ou, J. Effect of Fiber Reinforcement on Self-Healing Ability of Asphalt Mixture Induced by Microwave Heating. *Constr. Build. Mater.* **2023**, *362*, 129701. [CrossRef]
14. Gao, J.; Guo, H.; Wang, X.; Wang, P.; Wei, Y.; Wang, Z.; Huang, Y.; Yang, B. Microwave Deicing for Asphalt Mixture Containing Steel Wool Fibers. *J. Clean. Prod.* **2019**, *206*, 1110–1122. [CrossRef]
15. Shapie, S.S.; Taher, M.N.M. A Review of Steel Fiber's Potential Use in Hot Mix Asphalt. *IOP Conf. Ser. Earth Environ. Sci.* **2022**, *1022*, 012024. [CrossRef]
16. Liu, Q.; Li, B.; Schlangen, E.; Sun, Y.; Wu, S. Research on the Mechanical, Thermal, Induction Heating and Healing Properties of Steel Slag/Steel Fibers Composite Asphalt Mixture. *Appl. Sci.* **2017**, *7*, 1088. [CrossRef]
17. Du, Y.; Wang, J.; Deng, H.; Liu, Y.; Tian, J.; Wu, X. Using Steel Fibers to Accelerate the Heat Conduction in Asphalt Mixture and Its Performance Evaluation. *Constr. Build. Mater.* **2021**, *282*, 122637. [CrossRef]
18. Que, Z.; Tang, J.; Wei, H.; Zhou, A.; Wu, K.; Zou, D.; Yang, J.; Liu, T.; De Schutter, G. Predicting the Tensile Strength of Ultra-High Performance Concrete: New Insights into the Synergistic Effects of Steel Fiber Geometry and Distribution. *Constr. Build. Mater.* **2024**, *444*, 137822. [CrossRef]
19. Kim, J.-J.; Yoo, D.-Y. Effects of Fiber Shape and Distance on the Pullout Behavior of Steel Fibers Embedded in Ultra-High-Performance Concrete. *Cem. Concr. Compos.* **2019**, *103*, 213–223. [CrossRef]
20. Rezakhani, R.; Scott, D.A.; Bousikhane, F.; Pathirage, M.; Moser, R.D.; Green, B.H.; Cusatis, G. Influence of Steel Fiber Size, Shape, and Strength on the Quasi-Static Properties of Ultra-High Performance Concrete: Experimental Investigation and Numerical Modeling. *Constr. Build. Mater.* **2021**, *296*, 123532. [CrossRef]
21. Park, P.; El-Tawil, S.; Naaman, A.E. Pull-out Behavior of Straight Steel Fibers from Asphalt Binder. *Constr. Build. Mater.* **2017**, *144*, 125–137. [CrossRef]
22. García, A.; Norambuena-Contreras, J.; Partl, M.N.; Schuetz, P. Uniformity and Mechanical Properties of Dense Asphalt Concrete with Steel Wool Fibers. *Constr. Build. Mater.* **2013**, *43*, 107–117. [CrossRef]
23. Serin, S.; Morova, N.; Saltan, M.; Terzi, S. Investigation of Usability of Steel Fibers in Asphalt Concrete Mixtures. *Constr. Build. Mater.* **2012**, *36*, 238–244. [CrossRef]
24. Liu, Z.; Wang, Y.; Meng, Y.; Han, Z.; Jin, T. Comprehensive Performance Evaluation of Steel Fiber-Reinforced Asphalt Mixture for Induction Heating. *Int. J. Pavement Eng.* **2022**, *23*, 3838–3849. [CrossRef]
25. Abdallah, S.; Fan, M.; Cashell, K.A. Pull-out Behaviour of Straight and Hooked-End Steel Fibres under Elevated Temperatures. *Cem. Concr. Res.* **2017**, *95*, 132–140. [CrossRef]
26. Al-Osta, M.A.; Sharif, A.M.; Ahmad, S.; Adekunle, S.K.; Al-Huri, M.; Sharif, A.M. Effect of Hybridization of Straight and Hooked Steel Fibers and Curing Methods on the Key Mechanical Properties of UHPC. *J. Mater. Res. Technol.* **2021**, *15*, 3222–3239. [CrossRef]
27. Wang, L.; Deng, Z. Bond-Slip Response of End-Hook and Half-Hooked Steel Fibers in Moderately Strong SIFCON Matrix. *Constr. Build. Mater.* **2023**, *405*, 133334. [CrossRef]
28. Li, Y.; Liu, F.; Li, Q.; Li, H.; Sun, G.; Liang, R. Effect of Fiber Content and End Geometry on the Pullout Behavior of Straight and Arc-Shaped Steel Fibers Embedded in SIFCON. *Constr. Build. Mater.* **2024**, *451*, 138688. [CrossRef]
29. Li, Y.; Liu, F.; Li, H.; Pan, Y.; Liu, C. A Comparative Study on the Pullout Behavior of Hooked-End Straight and Arc-Shaped Steel Fibers from Brittle SIFCON Matrices under the Influence of Adjacent Fibers. *Constr. Build. Mater.* **2024**, *418*, 135311. [CrossRef]
30. *JTG F40-2004*; Technical Specifications for Highway Asphalt Pavement Construction. Industry Standard-Transportation: Beijing, China, 2004.
31. *JTG E20-2011*; Test Methods for Bitumen and Bituminous Mixtures for Highway Engineering. Industry Standard-Transportation: Beijing, China, 2011.

Disclaimer/Publisher's Note: The statements, opinions and data contained in all publications are solely those of the individual author(s) and contributor(s) and not of MDPI and/or the editor(s). MDPI and/or the editor(s) disclaim responsibility for any injury to people or property resulting from any ideas, methods, instructions or products referred to in the content.